

SIGMA: Scalable Spectral Insights for LLM Collapse

Yi Gu^{1*} Lingyou Pang^{2*} Xiangkun Ye³ Tianyu Wang⁴ Jianyu Lin⁴ Carey E. Priebe^{4†} Alexander Aue^{2†}

Abstract

The rapid adoption of synthetic data for training Large Language Models (LLMs) has introduced the technical challenge of “model collapse”—a degenerative process where recursive training on model-generated content leads to a contraction of distributional variance and representational quality. While the phenomenology of collapse is increasingly evident, rigorous methods to quantify and predict its onset in high-dimensional spaces remain elusive. In this paper, we introduce SIGMA (Spectral Inequalities for Gram Matrix Analysis), a unified framework that benchmarks model collapse through the spectral lens of the embedding Gram matrix. By deriving and utilizing deterministic and stochastic bounds on the matrix’s spectrum, SIGMA provides a mathematically grounded metric to track the contraction of the representation space. Crucially, our stochastic formulation enables scalable estimation of these bounds, making the framework applicable to large-scale foundation models where full eigendecomposition is intractable. We demonstrate that SIGMA effectively captures the transition towards degenerate states, offering both theoretical insights into the mechanics of collapse and a practical, scalable tool for monitoring the health of recursive training pipelines.

1. Introduction

LLM Collapse (Shumailov et al., 2024a;b) refers to the phenomenon where Large Language Models (LLMs) progressively degrade towards a degenerate state. This state arises as a result of recursive training, where models are

*Equal contribution †Alexander Aue and Carey E. Priebe jointly supervised this work and served as co-principal investigators. ¹Department of Mathematics, Northwestern University ²Department of Statistics, University of California, Davis ³Boston University ⁴Department of Applied Mathematics and Statistics, Johns Hopkins University. Correspondence to: Yi Gu <Yi.Gu@u.northwestern.edu>, Lingyou Pang <lyopang@ucdavis.edu>.

trained on iterations of data generated by other models, often previous versions of themselves. We term this model-generated output **Synthetic Data**, in contrast to organic data produced by human users.

In the current landscape of AI research, the demand for reliable and high-quality training data has never been higher. The scale of the latest generation of LLMs is increasing at such a staggering speed that the natural generation of internet content by humans cannot keep pace. Consequently, utilizing synthetic data has become a vital, if not inevitable, step in LLM training. While this is a logical progression, it carries a significant caveat. Without the infusion of new data produced by human users, model collapse occurs as the model iterates on its own probability distribution. Ultimately, the model may converge to a state characterized by low variance and degraded representational quality (Shumailov et al., 2024a;b).

Therefore, it is imperative to conduct a rigorous mathematical examination of LLM collapse. What are the underlying mechanisms at the mathematical level? How can this degradation be tracked and quantified throughout the training process? Furthermore, how can we leverage these metrics to gain deeper insights into LLM dynamics and guide the development of more efficient training architectures? This paper aims to answer these questions.

We introduce SIGMA (Spectral Inequalities for Gram Matrix Analysis), a novel framework that quantifies and benchmarks model collapse by utilizing the spectral bounds of the Gram matrix of LLM embedding vectors. The Gram matrix is a classical mathematical concept named after Jørgen Pedersen Gram. It has a wide range of applications in fields such as Riemannian geometry and control theory, and has found critical utility in modern applied mathematics and computer science domains, including the finite element method (Lanckriet et al., 2002). It is also widely used in classical NLP as an intuitive method to encode variable quantities of natural language embeddings into a fixed-dimensional matrix representation (Lodhi et al., 2002; Levy & Goldberg, 2014). As we enter the era of LLMs, the Gram matrix remains a vital tool, as it captures the intrinsic geometry and distributional properties of the data we seek to analyze. SIGMA revisits this fundamental operator to quantify the modern phenomenon of representa-

tion collapse.

Inevitably, the spectrum of the Gram matrix becomes the key to understanding LLM collapse. We develop our theory and framework around this central mathematical object, allowing us to monitor, estimate, and predict the behavior of LLMs regarding model collapse through training iterations. Crucially, our method utilizes both deterministic and stochastic bounds to function effectively even with partially observed data, ensuring our framework remains scalable for large-scale models.

Our contributions can be summarized as follows:

- **A Theoretical Framework for Collapse Detection:** We propose SIGMA, a spectral analysis framework that rigorously links the decay of the Gram matrix eigenspectrum to the phenomenon of model collapse.
- **Rigorous Spectral Bounds:** We derive both deterministic and stochastic inequalities for the Gram matrix, allowing for precise estimation of representation collapse even in high-dimensional settings where exact computation is prohibitively expensive.
- **Scalable Benchmarking Metrics:** Leveraging these bounds, we introduce a set of scalable metrics that can track the “health” of an LLM’s distribution during recursive training, providing an early warning system for the onset of degenerate states.

2. Background

2.1. Related Work

The risk of training generative models on their own outputs has been formalized as *model collapse*, where repeated self-training progressively erodes distributional support, particularly in the tails, and can culminate in highly generic or degenerate generations (Shumailov et al., 2024a;b).

Related phenomena have been studied under different labels and experimental protocols, including *Model Autophagy Disorder* (MAD), which emphasizes precision–recall trade-offs and the role of “fresh” real data injections across generations (Alemohammad et al., 2023). Recent theory sharpens these concerns by distinguishing regimes where degradation is transient versus *strong* and asymptotic, even when synthetic data is mixed with a constant fraction of real data (Dohmatob et al., 2024).

Complementary analyses interpret recursion as an entropy- or variance-contracting process and propose tail-centric quantities such as time-to-forget and covariance shrinkage to explain why rare events vanish first (Seddk et al., 2024). Other lines formalize stability of self-consuming loops via recursion-stability notions, connecting collapse

to unbounded generalization degradation across generations (Yoon et al., 2025).

Finally, practical collapse signals in text include over-concentration of surface features (e.g., n -grams), emphasizing the need for diagnostics that are sensitive to diversity loss beyond average quality metrics (Zhu et al., 2025). Most prior work studies recursion within a single-model loop (or a fixed teacher–student chain), whereas real-world synthetic data arises from multi-model, retrieval-mediated ecosystems. Building on this black-box perspective, recent work develops statistically grounded uncertainty and calibration techniques tailored to LLM-as-a-Judge systems (Pang et al., 2025b;a), and studies related dynamics that can shift judge behavior over time (Wang et al., 2025), where LLM Web Dynamics (LWD) explicitly targeting this setting by modeling a network of LLMs coupled through a retrieval-augmented substrate, and analyzes convergence patterns under such web-like feedback.

In contrast to task- or token-level statistics alone, our SIGMA framework focuses on *representation geometry*: we track collapse via the eigenspectrum of embedding Gram matrices and develop deterministic and stochastic spectral inequalities that enable scalable, one-sided monitoring when only partial Gram information is available.

2.2. Preliminaries

For initial information encoding in LLMs, the i -th sentence is mapped to a vector of a fixed dimension m . We denote this vector as $X_i \in \mathbb{R}^m$, which is referred to as the *embedding* or the *embedding vector* of the sentence. Let the set of embedding vectors be $E_0 = \{X_i : i \in [n]\}$, where $[n] := \{1, \dots, n\}$. E_0 represents our starting evaluation corpus. We operate under the regime where the sample size exceeds the embedding dimension, i.e., $n > m$.

Subsequently, we construct an $m \times n$ matrix M by concatenating all embedding vectors column-wise. We define the Gram matrix as:

$$G = MM^\top, \quad (2.1)$$

with respect to the set E_0 . Note that G is an $m \times m$ matrix whose dimensions are independent of the sample size $|E_0|$, though its entries depend on the samples. Since we assume $n > m$, it is possible for G to be full rank. Given that LLMs are probabilistic models, the set E contains random vectors; consequently, G is treated as a random matrix. Our objective is to establish a benchmark using the spectrum of the Gram matrix to measure the magnitude of *model collapse*.

It is well known that the Gram matrix G captures the inter-dependency relations between the semantic features of the sentences. We posit that G being full rank is a necessary condition for the LLM to function properly, indicating that

the model utilizes the full capacity of its embedding space. Conversely, if G is singular (or effectively rank-deficient), it implies information loss at the semantic level and marks the onset of model collapse.

To provide an intuitive (non-rigorous) example: imagine a collapsed LLM that outputs identical or highly repetitive phrasing for distinct queries. These outputs would map to linearly dependent embedding vectors, failing to span the ambient space \mathbb{R}^m , thereby resulting in a singular Gram matrix.

Motivated by this, we introduce the log-determinant as our primary benchmark metric for model collapse:

$$\log |G| = \log \left(\prod_{j=1}^m \lambda_j \right) = \sum_{j=1}^m \log(\lambda_j), \quad (2.2)$$

where λ_j are the eigenvalues of G . When collapse occurs, we expect a sharp decrease in the log-determinant (diverging towards $-\infty$ as $\lambda_{\min} \rightarrow 0$).

3. The SIGMA Framework: Deterministic & Spectral Bounding of the Gram Matrix

To rigorously quantify model collapse, we analyze the spectral properties of the embedding Gram matrix. However, computing the full spectrum for large-scale LLMs is often computationally intractable due to the sheer volume of tokens (n_k) relative to the embedding dimension (m). In this section, we present the SIGMA framework, which leverages a sub-sampling strategy to derive both deterministic and stochastic bounds on the Gram determinant. This allows us to estimate the “health” of the representation space using only a fraction of the data.

3.1. Setup and Notations

We track the model’s state at a fixed training iteration k . Adding superscripts to the basic notation in (2.2), let $M^{(k)} \in \mathbb{R}^{m \times n_k}$ be the embedding matrix, where each column $v_j^{(k)} \in \mathbb{R}^m$, $1 \leq j \leq n_k$ is an embedding vector. We define the *Gram matrix* as:

$$G^{(k)} := M^{(k)} \left(M^{(k)} \right)^\top = \sum_{j=1}^{n_k} v_j^{(k)} \left(v_j^{(k)} \right)^\top \in \mathbb{S}_+^m, \quad (3.1)$$

where \mathbb{S}_+^m denotes the set of $m \times m$ positive semi-definite matrices. We denote the eigenvalues of $G^{(k)}$ by $\lambda_1(G^{(k)}) \geq \dots \geq \lambda_m(G^{(k)}) \geq 0$.

The Sub-Sampling Strategy. Since n_k is typically massive,

we partition the embedding matrix $M^{(k)}$ into two blocks:

$$A^{(k)} \in \mathbb{R}^{m \times n_A}: \text{The observed block};$$

$$B^{(k)} \in \mathbb{R}^{m \times n_B}: \text{The unobserved block}.$$

Here, $n_k = n_A + n_B$, and we assume $n_A > m$ to ensure rank stability. $A^{(k)}$ consists of the columns we keep during the computation and $B^{(k)}$ contains the part we ignore. Write

$$G_A^{(k)} = A^{(k)}(A^{(k)})^\top, \quad G_B^{(k)} = B^{(k)}(B^{(k)})^\top \quad (3.2)$$

the **sub-Gram Matrices** formed by $A^{(k)}$ and $B^{(k)}$. A simple computation gives us

$$G^{(k)} = G_A^{(k)} + G_B^{(k)}. \quad (3.3)$$

Our goal is to bound the spectrum (and determinant) of the full $G^{(k)}$ using only the observable $G_A^{(k)}$.

3.2. Main Results

We first provide a rigorous deterministic bound that relies on no distributional assumptions, utilizing Weyl’s inequality and Ky Fan dominance. The detailed deduction as well as the proofs of theorems can be found in appendix A.

Theorem 1 (Deterministic Spectral Bound). *Let $G^{(k)} = G_A^{(k)} + G_B^{(k)}$ be as defined above. Let $\beta_k := \lambda_{\max}(G_B^{(k)})$ be the spectral radius of the unobserved component. Then, the determinant of the full Gram matrix is bounded by:*

$$\det(G_A^{(k)}) \leq \det(G^{(k)}) \leq \prod_{i=1}^m \left(\lambda_i(G_A^{(k)}) + \beta_k \right). \quad (3.4)$$

While Theorem 1 is rigorous, the dependence on β_k (the max eigenvalue of the unobserved data) makes it loose in practice. To obtain a scalable estimator for real-world monitoring, we derive a stochastic bound assuming the data is drawn from a consistent underlying distribution. This assumption does not restrict the geometric complexity of the embeddings; it merely posits that the generative process is stationary, ensuring that the spectral properties of the sub-sample generalize to the full corpus.

Theorem 2 (Stochastic Scaling Spectral Bound). *Assume the columns of $M^{(k)}$ are i.i.d. samples drawn from a distribution with covariance matrix $C \in \mathbb{S}_+^m$. As $n_A, n_k \rightarrow \infty$ with fixed m , there exists a finite constant K such that with high probability:*

$$\det(G^{(k)}) \approx \left(\frac{n_k}{n_A} \right)^m \det(G_A^{(k)}). \quad (3.5)$$

Specifically, the upper bound holds in expectation:

$$\mathbb{E}[\det(G^{(k)})] \leq K \cdot \left(\frac{n_k}{n_A} \right)^m \det(G_A^{(k)}). \quad (3.6)$$

Theorem 2 implies a **simple operational scaling law**: for a healthy model, the log-determinant increases naturally with sample size as $m \log n_k$. This allows us to define a *size-invariant* baseline: the difference $\log \det G^{(k)} - m \log n_k$ should remain constant across checkpoints. By monitoring this corrected value, we isolate genuine geometric collapse from trivial fluctuations in dataset size, ensuring that any observed negative drift reflects a true degradation in the model's representational capacity.

3.3. Error Estimation

Naturally, we will be interested in how much error does the theorems in the previous section introduce. In fact, 2 provides extra insights for the tightness of inequalities in 1. Let C be the covariance matrix defined in theorem 2. We know that for large n_A, n_k , $\det(G^{(k)}) \approx (n_k/n_A)^m \det(G_A^{(k)}) \approx n^m \det(C)$, we can define the asymptotic **Overestimation Ratio** \mathcal{R} as the ratio of the Weyl bound to the stochastic expected value:

$$\begin{aligned} \mathcal{R} &= \frac{1}{\det G^{(k)}} \prod_{i=1}^m \left(\lambda_i(G_A^{(k)}) + \beta_k \right) \\ &\approx \prod_{j=1}^m \frac{n_A \lambda_j(C) + (n_k - n_A) \lambda_{\max}(C)}{n \lambda_j(C)}. \end{aligned} \quad (3.7)$$

Dividing through by n , and letting $\rho = n_A/n$, we have a more concise formula

$$\mathcal{R} \approx \prod_{j=1}^m \left(\rho + (1 - \rho) \frac{\lambda_{\max}(C)}{\lambda_j(C)} \right). \quad (3.8)$$

For each j , we consider the ratio $\lambda_{\max}(C)/\lambda_j(C) \geq 1$. If this ratio is close to 1 for all j , it implies the covariance matrix C is close to being *isotropic*; consequently, the overestimation ratio will also be close to 1, yielding an asymptotically tight deterministic bound.

On the other hand, if C is more *anisotropic* - i.e., the ratio $\lambda_{\max}(C)/\lambda_j(C) \gg 1$ for some smaller eigenvalues $\lambda_j(C)$ - then the term $(1 - \rho) \lambda_{\max}(C)/\lambda_j(C)$ will dominate the product in (3.8) and cause the error to grow.

As for theorem 2 itself, we can also give a more refined estimation of the error. Let X be a random vector drawn from the i.i.d. distribution in theorem 2, we set

$$\sigma := \text{Var}(X^T C X). \quad (3.9)$$

The following theorem holds:

Theorem 3 (Stochastic Error Term). *Assume the settings of theorem 1 and, in addition, the distribution of column vectors has a finite fourth moment. Then as $n_A, n_k \rightarrow \infty$*

with $n_A < n_k$, we have

$$\frac{\log \det G^{(k)} - \log \det G_A^{(k)} - m \log(n_k/n_A)}{\sigma \sqrt{\frac{1}{n_A} - \frac{1}{n_k}}} \rightarrow \mathcal{N}(0, 1) \quad (3.10)$$

in distribution. Consequently, for any $\alpha \in (0, 1)$, let $z_{\alpha/2} = \Phi^{-1}(1 - \alpha/2)$. Then with probability approaching $1 - \alpha$:

$$\begin{aligned} &\left| \log \det G_n - \log \left(\left(\frac{n_k}{n_A} \right)^m \det G_A \right) \right| \\ &\leq z_{\alpha/2} \cdot \sigma \sqrt{\frac{1}{n_A} - \frac{1}{n_k}}. \end{aligned} \quad (3.11)$$

Stability in Large Corpora. While theorem 2 establishes the asymptotic scaling law, theorem 3 quantifies the precision of this law in finite samples. Specifically, it provides the exact confidence intervals required to bound the error of our scaling-law estimator in the finite-sample regime. The estimation error depends on the factor $\sqrt{1/n_A - 1/n_k}$. In the practical regime where the total volume of model outputs is massive compared to our observed sample ($n_k \gg n_A$), this factor simplifies effectively to

$$\sqrt{\frac{1}{n_A} - \frac{1}{n_k}} \approx \frac{1}{\sqrt{n_A}}. \quad (3.12)$$

This leads to a crucial practical insight: the precision of our collapse monitoring depends primarily on the *size of our observed block* n_A , not on the total size of the unobserved corpus. Even if the total output n_k grows indefinitely, our estimate remains stable.

This motivates the definition of a simple plug-in estimator for the full log-determinant:

$$\widehat{L}^{(k)} := \log \det G_A^{(k)} + m \log \left(\frac{n_k}{n_A} \right). \quad (3.13)$$

Using the rigorous result from (3.11), we derive a practical rule-of-thumb for large datasets ($n_k \gg n_A$) with $(1 - \alpha)$ confidence interval:

$$\log \det G^{(k)} \approx \widehat{L}^{(k)} \pm \frac{z_{\alpha/2} \sigma}{\sqrt{n_A}}. \quad (3.14)$$

This formula allows practitioners to easily determine the necessary sample size: to achieve a target precision ε , one simply needs to choose an observed block size of $n_A \gtrsim (z_{\alpha/2} \sigma / \varepsilon)^2$.

3.4. SIGMA-UB Collapse Monitoring

Section 3.2 establishes the theoretical foundation for detection, but the raw bounds rely on unobserved quantities ($G_B^{(k)}$) or unknown constants (K). This subsection translates

those theorems into two scalar, fully computable diagnostics, computed only from $(G_A^{(k)}, n_A, n_k)$.

Regularization Convention (δ). We fix a small constant $\delta > 0$ and evaluate log-volumes using $\log \det(\cdot + \delta I_m)$. The same δ is reused across all checkpoints to ensure comparability and numerical stability under rank deficiency. This regularization ensures the metric is well-defined and Lipschitz continuous with respect to small perturbations in the embeddings.

Now we turn both theorem 1 and theorem 2 into **computationally scalable monitoring metrics** via the following two bridges, respectively.

Diagnostic I (Theorem 1): Tail-Energy Budget. Note that we never construct $B^{(k)}$ and thus cannot measure β_k . Instead, we enforce a standard embedding preprocessing (e.g., ℓ_2 -normalization or clipping) so that $\|v_j^{(k)}\|_2^2 \leq \rho$ for all generated responses. With $n_2 := n_k - n_A$ unseen columns, this yields the computable worst-case budget

$$\hat{\beta}_k := (n_k - n_A) \rho. \quad (3.15)$$

Appendix B shows that substituting $\hat{\beta}_k$ produces a valid one-sided envelope for the full regularized log-determinant.

Diagnostic II (Theorem 2): Constant-Free Size Correction. Recall that Theorem 2 implies the full model entropy is effectively the sub-sample entropy shifted by the geometric scaling factor $m \log(n_k/n_A)$. While the exact value depends on an unknown constant K , we can eliminate this constant by monitoring the trend rather than the absolute value.

Combining this with Theorem 1, we operationally track collapse via two complementary diagnostics: (i) a size-corrected statistic that relies on this stochastic scaling, and (ii) a normalized deterministic envelope that uses a computable tail budget.

Two Computable Diagnostics. We monitor collapse using (i) a normalized deterministic envelope and (ii) a covariance-normalized LLN proxy:

$$\begin{aligned} \mathcal{G}_{\text{KF}}^{(k)}(\delta) &:= \log \det(G_A^{(k)} + (\hat{\beta}_k + \delta) I_m) \\ &\quad - m \log(\hat{\beta}_k + \delta), \end{aligned} \quad (3.16)$$

$$\mathcal{U}_{\text{LLN},\text{cov}}^{(k)}(\delta) := \log \det(G_A^{(k)} + \delta I_m) - m \log n_A. \quad (3.17)$$

We report baseline drifts

$$\begin{aligned} \Delta \mathcal{G}_{\text{KF}}^{(k)}(\delta) &:= \mathcal{G}_{\text{KF}}^{(k)}(\delta) - \mathcal{G}_{\text{KF}}^{(0)}(\delta), \\ \Delta \mathcal{U}_{\text{LLN},\text{cov}}^{(k)}(\delta) &:= \mathcal{U}_{\text{LLN},\text{cov}}^{(k)}(\delta) - \mathcal{U}_{\text{LLN},\text{cov}}^{(0)}(\delta). \end{aligned} \quad (3.18)$$

SIGMA-UB Monitoring Algorithm. Algorithm 1 computes both diagnostics at each checkpoint using only the sub-Gram

Algorithm 1 SIGMA-UB Collapse Monitoring (upper-bound diagnostics)

Require: $\{G_A^{(k)}\}_{k=0}^K$, counts $\{n_k\}_{k=0}^K$, fixed n_A , and hyperparameters $\delta > 0$, $\rho > 0$.

- 1: Define $\text{LOGDET}_\delta(X) := \log \det(X + \delta I_m)$.
- 2: **for** $k = 0, \dots, K$ **do**
- 3: $\hat{\beta}_k \leftarrow (n_k - n_A) \rho$
- 4: $S_k \leftarrow \text{LOGDET}_\delta(G_A^{(k)})$
- 5: $\mathcal{G}_{\text{KF}}^{(k)} \leftarrow \text{LOGDET}_\delta(G_A^{(k)} + \hat{\beta}_k I_m) - m \log(\hat{\beta}_k + \delta)$
- 6: $\mathcal{U}_{\text{LLN},\text{cov}}^{(k)} \leftarrow S_k - m \log n_A$
- 7: **if** $k = 0$ **then**
- 8: store $(\mathcal{G}_{\text{KF}}^{(0)}, \mathcal{U}_{\text{LLN},\text{cov}}^{(0)})$
- 9: **else**
- 10: compute drifts $\Delta \mathcal{G}_{\text{KF}}^{(k)}, \Delta \mathcal{U}_{\text{LLN},\text{cov}}^{(k)}$ via (3.18)
- 11: **end if**
- 12: **end for**

Return: $\Delta \mathcal{G}_{\text{KF}}^{(K)}, \Delta \mathcal{U}_{\text{LLN},\text{cov}}^{(K)}$

matrix and counts. In practice, $\log \det(\cdot)$ is computed via Cholesky on the shifted PSD matrix (Appendix B).

How to Interpret the Outputs. Both diagnostics decrease when eigenvalues of $G_A^{(k)}$ contract, with heightened sensitivity near the δ floor. Operationally, a sustained negative drift in either $\Delta \mathcal{G}_{\text{KF}}^{(k)}(\delta)$ or $\Delta \mathcal{U}_{\text{LLN},\text{cov}}^{(k)}(\delta)$ signals collapse onset; saturation indicates late-stage rank collapse. The two-track design is intentional: $\Delta \mathcal{G}_{\text{KF}}$ is a deterministic, conservative envelope controlled by a known tail-energy budget, while $\Delta \mathcal{U}_{\text{LLN},\text{cov}}$ is a sensitive size-corrected proxy whose unknown constants cancel under differencing. Disagreement between the tracks is itself informative, often indicating violations of the consistent-context assumption (prompt drift, retrieval drift, filtering changes) rather than numerical artifacts.

4. Experiments

4.1. Experiment Objectives and Controlled Assets

Our experiments measure the operational behavior of training with recursively regenerated synthetic text under tightly controlled, evaluation-stable conditions. We isolate two questions, aligned with two settings (S1–S2):

(1) Data recursion (S1). When synthetic text is regenerated every generation but each training run *restarts from the same base checkpoint*, do the SIGMA geometry diagnostics drift progressively, indicating representational contraction driven purely by *data feedback*?

(2) Weight recursion (S2). Under the *same* regeneration protocol and real:synth mixture rule, does *carrying model weights across generations* materially amplify or alter col-

lapse dynamics relative to restart-from-base training?

Assets and evaluation stability. We reuse the *license-clean real corpora* and *frozen prompt banks* from DecayBench as controlled assets. Each domain

$$d \in \{\text{CIVICS, FINANCE, SCIENCE, SOFTWARE}\}$$

provides: (i) a real corpus $R^{(d)}$ pre-sliced into non-overlapping 64-token contexts, and (ii) a fixed prompt bank $P^{(d)}$ with stable prompt IDs (and bucket labels). To avoid evaluation drift, *all* checkpoints are evaluated on the same frozen prompt bank $P^{(d)}$ with fixed decoding and a frozen sentence encoder. Following the main-text budget, we report results on a single target domain (FIN) and provide full numeric tables and auxiliary analyses in Appendix C.

4.2. Models and Fine-Tuning Setup

Unless otherwise noted, we start from a single base checkpoint $M^{(0)}$ (e.g., OPT-125M) and fine-tune with a fixed optimizer, training budget, and data formatting across all conditions. All training examples are stored as 64-token text blocks so that token budgets remain comparable. Full hyperparameters and run metadata (optimizer/LR, steps, batch size, weight decay, decoding, seeds) are consolidated in an experiment card (Appendix C.2).

4.3. Synthetic Generation, Mixture Rule, and Two Recursion Settings

Regeneration protocol and constant-budget mixtures.

For a fixed domain d , we use each real 64-token context $x \in R^{(d)}$ as a prompt and sample a fixed-length continuation from the previous-generation model to form a synthetic pool $S^{(g,d)}$ at generation $g \geq 1$. Training data at generation g is a constant-budget mixture of *synthetic* and *real* examples: a fraction $(1 - \alpha)$ are drawn from $S^{(g,d)}$ and a fraction α from $R^{(d)}$, with the total number of training blocks held fixed to $|R^{(d)}|$. The real fraction $\alpha \in [0, 1]$ is held fixed within each run.

Setting S1: restart-from-base (data recursion only). Each generation regenerates a fresh synthetic pool, but training always restarts from the same base checkpoint:

$$M^{(g,d)} \leftarrow \text{Finetune}(M^{(0)}, D^{(g,d)}(\alpha)).$$

This isolates collapse induced by the *evolving synthetic data distribution* without compounding weight updates across generations.

Setting S2: true recursion (data + weight recursion). This setting carries weights across generations under the same regeneration and mixture rule:

$$M^{(g,d)} \leftarrow \text{Finetune}(M^{(g-1,d)}, D^{(g,d)}(\alpha)).$$

Comparing S1 vs. S2 therefore isolates the *incremental effect of weight recursion* under a matched synthetic regeneration pipeline.

4.4. Collapse Measurements and Baselines

SIGMA-UB (two-track geometry diagnostics). At each evaluated checkpoint (generation g in S1/S2), we generate one response per frozen prompt (fixed decoding), embed responses with a *frozen* sentence encoder, and compute the two SIGMA-UB diagnostics from Section 3.4 (Algorithm 1) on a *fixed* observed index set (shared across checkpoints within a run). We report baseline drifts relative to the base checkpoint ($g = 0$): (i) Track II $\Delta U_{\text{LLN},\text{cov}}(\delta)$ and (ii) Track I $\Delta G_{\text{KF}}(\delta)$.

Interpretation. More negative drift indicates stronger contraction of the observed sub-Gram spectrum. Track II is the sensitive trend probe (observed-spectrum contraction); Track I is a conservative guardrail and may be loose when dominated by the worst-case tail-energy budget. We therefore interpret the *joint* behavior of both tracks as the primary diagnostic signal.

Surface-form proxies (non-definitional). To contextualize geometry drift, we also compute lightweight surface-form diversity proxies (distinct-2 and hashed n -gram HHI) on the same model outputs used for SIGMA-UB. Full proxy reporting is deferred to Appendix C.4.

4.5. Main-Text Reporting: Two Plots and One Table (FIN)

To keep the main text minimal and directly comparable across settings, we report: (i) two plots—one for S1 and one for S2—each showing both SIGMA-UB tracks, and (ii) one compact table summarizing S1 vs. S2 via final drift and an OLS slope over generations. All underlying per-generation values used to render the plots and compute the summary scalars are provided in Appendix C.3.

Result (S1 vs. S2). On FIN, restart-from-base recursion (S1) shows a mild but consistently negative drift under both tracks by $g_{\text{max}} = 50$ (final drifts ≈ -151 and ≈ -142), consistent with gradual contraction driven by the evolving synthetic pool. Under true recursion (S2), Track II exhibits a much larger negative drift (final ≈ -1537 ; slope ≈ -42.6), indicating substantially accelerated contraction when weights are carried across generations. In contrast, Track I remains near-zero and can even trend slightly positive over the same window, reflecting that the KF envelope is governed by a worst-case tail-energy budget rather than the observed spectrum itself; this Track II/Track I separation is an intended diagnostic feature of SIGMA-UB.

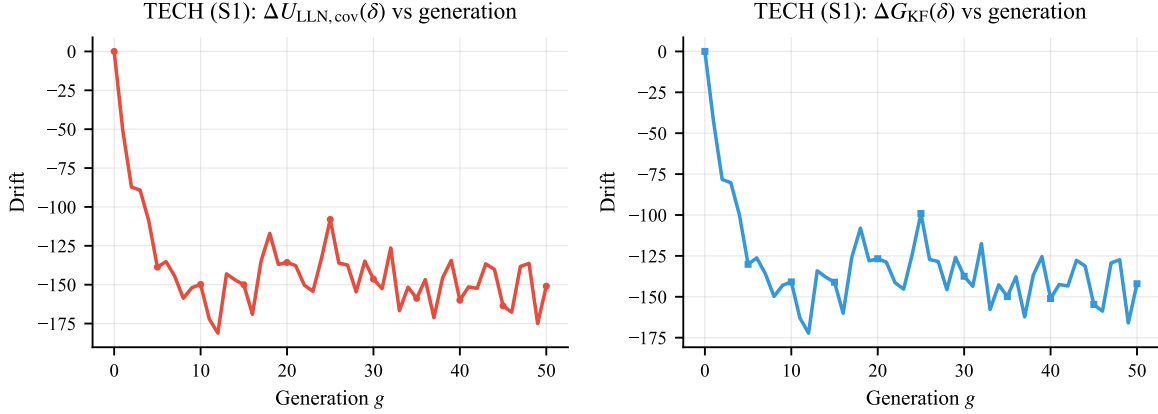


Figure 1. FIN, Setting S1 (restart-from-base): drift vs. generation under both SIGMA-UB tracks. Top: Track II $\Delta U_{LLN,cov}(\delta)$. Bottom: Track I $\Delta G_{KF}(\delta)$. Values are baseline drifts relative to the base checkpoint ($g = 0$). S1 isolates *data recursion only*: synthetic text is regenerated each generation, but training restarts from the same base checkpoint. Appendix C.3 reports the exact per-generation table used to render this figure.

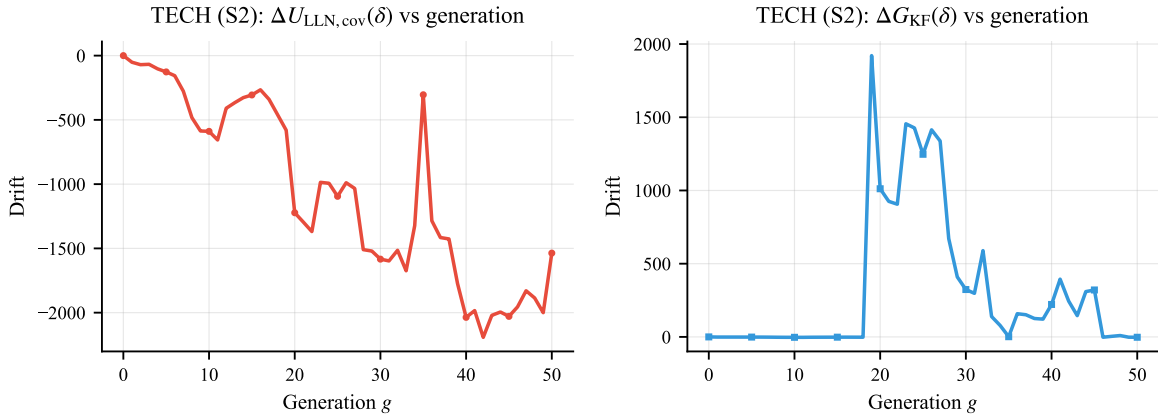


Figure 2. FIN, Setting S2 (true recursion): drift vs. generation under both SIGMA-UB tracks. Top: Track II $\Delta U_{LLN,cov}(\delta)$. Bottom: Track I $\Delta G_{KF}(\delta)$. Values are baseline drifts relative to the base checkpoint ($g = 0$). S2 compounds *data recursion + weight recursion*: each generation regenerates synthetic text and continues training from the previous generation weights. Appendix C.3 reports the exact per-generation table used to render this figure.

Acknowledgements

The first author would like to thank his friend Xiaoyu Li for his unwavering support throughout the difficult times.

References

Alemohammad, S., Casco-Rodriguez, J., Luzi, L., Hu-mayun, A. I., Babaei, H., LeJeune, D., Siahkoohi, A., and Baraniuk, R. G. Self-consuming generative models go mad, 2023. URL <https://arxiv.org/abs/2307.01850>.

Dohmatob, E., Feng, Y., Subramonian, A., and Kempe, J. Strong model collapse, 2024. URL <https://arxiv.org/abs/2410.04840>.

Lanckriet, G. R. G., Cristianini, N., Bartlett, P., El Ghaoui, L., and Jordan, M. I. Learning the kernel matrix with semi-definite programming. Technical report, University of California, USA, 2002.

Levy, O. and Goldberg, Y. Neural word embedding as implicit matrix factorization. In Ghahramani, Z., Welling, M., Cortes, C., Lawrence, N., and Weinberger, K. (eds.), *Advances in Neural Information Processing Systems*, volume 27. Curran Associates, Inc., 2014.

Lodhi, H., Saunders, C., Shawe-Taylor, J., Cristianini, N., and Watkins, C. Text classification using string kernels. *J. Mach. Learn. Res.*, 2:419–444, March 2002. ISSN 1532-4435. doi: 10.1162/153244302760200687.

Pang, L., Huang, L., Lin, J., Wang, T., Aue, A., and Priebe,

Setting	g_{\max}	$\Delta U_{\text{LLN},\text{cov}}$ (final)	$\text{slope}_{\text{LLN},\text{cov}}$	ΔG_{KF} (final)	slope_{KF}	Track agreement?
S1	50	-150.986	-0.941	-142.051	-0.918	yes (both negative)
S2	50	-1536.562	-42.621	-2.426	2.350	no (Track II collapses; Track I does not)

Table 1. FIN summary statistics (S1 vs. S2). We summarize each drift curve using: (i) *final drift* at the last available generation g_{\max} , and (ii) an ordinary least-squares *slope* of drift versus generation (more negative implies faster degradation over the observed window; slopes are fit on the full drift series including the $g=0$ baseline point). Track agreement reports whether both tracks trend negative (qualitative agreement) or whether Track II indicates strong contraction without a matching Track I response. Appendix C.3 provides the per-generation tables used to compute these scalars.

C. E. Taming variability: Randomized and bootstrapped conformal risk control for llms, 2025a. URL <https://arxiv.org/abs/2509.23007>.

Pang, L., Huang, L., Lin, J., Wang, T., Horiguchi, A., Aue, A., and Priebe, C. E. Unsupervised conformal inference: Bootstrapping and alignment to control llm uncertainty, 2025b. URL <https://arxiv.org/abs/2509.23002>.

Seddik, M. E. A., Chen, S.-W., Hayou, S., Youssef, P., and Debbah, M. How bad is training on synthetic data? a statistical analysis of language model collapse, 2024. URL <https://arxiv.org/abs/2404.05090>.

Shumailov, I., Shumaylov, Z., Zhao, Y., Gal, Y., Papernot, N., and Anderson, R. The curse of recursion: Training on generated data makes models forget, 2024a. URL <https://arxiv.org/abs/2305.17493>.

Shumailov, I., Shumaylov, Z., Zhao, Y., Papernot, N., Anderson, R., and Gal, Y. AI models collapse when trained on recursively generated data. *Nature*, 631(8022):755–759, July 2024b.

Wang, T., Horiguchi, A., Pang, L., and Priebe, C. E. Llm web dynamics: Tracing model collapse in a network of llms, 2025. URL <https://arxiv.org/abs/2506.15690>.

Yoon, Y., Hu, D., Weissburg, I., Qin, Y., and Jeong, H. Model collapse in the self-consuming chain of diffusion finetuning: A novel perspective from quantitative trait modeling, 2025. URL <https://arxiv.org/abs/2407.17493>.

Zhu, X., Cheng, D., Li, H., Zhang, K., Hua, E., Lv, X., Ding, N., Lin, Z., Zheng, Z., and Zhou, B. How to synthesize text data without model collapse?, 2025. URL <https://arxiv.org/abs/2412.14689>.

A. Mathematical Deductions and Proof of Theorems

We Adopt the notations from section 3.1, for the Gram matrix $G^{(k)}$, if $\text{rank}(M^{(k)}) < m$ (e.g., if $n_k < m$ or the columns of $M^{(k)}$ are linearly dependent), then $G^{(k)}$ is singular and $\det(G^{(k)}) = 0$. In practice, we usually have $n_k \gg m$, and the Cauchy–Binet formula for Gram matrices yields

$$\det(G^{(k)}) = \sum_{J \subset [n_k], |J|=m} \det(M_J^{(k)})^2, \quad (\text{A.1})$$

where $M_J^{(k)}$ is the $m \times m$ submatrix formed by columns indexed by J . Recall from Section 2.2 that computing the full Gram matrix can be computationally prohibitively expensive. Instead, we compute the log-determinant of the sub-Gram matrix, formed by selecting a subset of the columns in the embedding matrix.

Proof of Theorem 1. To prove the lower bound, notice that $A^{(k)}$ is a sub-matrix of $M^{(k)}$. By the Cauchy Binet formula (A.1), the sum defining $\det(G_A^{(k)})$ is a subset of the sum defining $\det(G^{(k)})$. This directly implies

$$\det(G_A^{(k)}) \leq \det(G^{(k)}). \quad (\text{A.2})$$

For the second half of the inequality, we use Weyl’s inequality and Ky Fan dominance and for each i :

$$\lambda_i(G^{(k)}) \leq \lambda_i(G_A^{(k)}) + \lambda_1(G_B^{(k)}). \quad (\text{A.3})$$

Hence, with $\beta_k := \lambda_{\max}(G_B^{(k)})$, we have:

$$G^{(k)} \preceq G_A^{(k)} + \beta_k I_m, \quad \det(G^{(k)}) \leq \prod_{i=1}^m (\lambda_i(G_A^{(k)}) + \beta_k). \quad (\text{A.4})$$

Combining the lower bound in (A.2) and the upper bound in (A.4) yields the stated result. \square

The Cauchy-Binet formula, as well as the bound in Eq. (A.4), opens a window for us to bound the determinant of the original Gram matrix. Alas, the upper bound is not sharp because there is no way for us to extract information from the columns that we do not choose.

However, in practice, this is usually not the case because the dataset we are working on typically comes from a consistent context. If we use the analogy of viewing the Gram matrix as a book, then the chapters we read (i.e., $G_A^{(k)}$) are usually a good indication of the chapters we do not read (i.e., $G_B^{(k)}$), even though mathematically the unseen chapters could contain content that is completely irrelevant.

To reflect such realistic circumstances, we assume that the embedding column vectors are drawn from an implicit distribution (probability measure) μ . Denote v as an arbitrary column (where v can be seen as a random variable) and let $C = \mathbb{E}[vv^\top]$ be the covariance matrix. With this additional assumption, We proceed with the asymptotic argument.

Proof of Theorem 2. By the Strong Law of Large Numbers,

$$\frac{1}{n_k} G^{(k)} \rightarrow C \quad \text{a.s.} \quad (\text{A.5})$$

For the original Gram matrix, since n_k is usually very large, we have

$$\det(G^{(k)}) \approx \det(n_k C) = n_k^m \det(C). \quad (\text{A.6})$$

On the other hand, assuming n_A is sufficiently large to approximate the population covariance, then

$$\det(G_A^{(k)}) \approx O(\det(n_A C)) = n_A^m \det(C). \quad (\text{A.7})$$

Therefore, we have a stochastic upper bound of the original Gram matrix using the sub-Gram matrix: there exists a finite constant $K < \infty$ such that for each iteration k ,

$$\det(G^{(k)}) \leq K \cdot \left(\frac{n_k}{n_A} \right)^m \det(G_A^{(k)}). \quad (\text{A.8})$$

\square

This bound serves as an asymptotic scaling law rather than a point-wise estimator of $\det(G^{(k)})$. It gives us a theoretical foundation for monitoring model collapse with partial data, assuming the bare minimum: that the data we are processing comes from a consistent context.

Proof of Theorem 3. Since we assume that the distribution of column vectors have a finite fourth moment, we know

$$Z := X^T C^{-1} X = \sum_{i,j=1}^m X_i X_j \quad (\text{A.9})$$

has a finite variance. i.e., σ is finite. In fact, Z is the Mahalanobis distance. It plays an important role in this proof. For lighter notation, we write $n \equiv n_k$ and $G_t \equiv G_t^{(k)}$ the gram matrix formed by selecting t columns from $M^{(k)}$. This way $G^{(k)} \equiv G_n$ and $G_A^{(k)} \equiv G_{n_A}$. Notice that

$$\det(G_{t+1}) = \det(G_t)(1 + X_{t+1}^T G_t^{-1} X_{t+1}). \quad (\text{A.10})$$

Denote $L_n = \log \det G_n$ and we get

$$L_n - L_{n_A} = \sum_{t=n_A}^{n-1} \log (1 + X_{t+1}^T G_t^{-1} X_{t+1}). \quad (\text{A.11})$$

Write the normalized deviation matrix as $\Delta_t := tG_t^{-1} - C^{-1}$. We need the following lemma:

Lemma 4 (Convergence Rate of Deviation Matrix). *Under the assumption of finite fourth moments, the operator norm of the deviation matrix satisfies $\|\Delta_t\|_{op} = O_p(t^{-1/2})$.*

Proof of Lemma 4. Let $\hat{C}_t = \frac{1}{t} G_t = \frac{1}{t} \sum_{i=1}^t X_i X_i^T$. Since the random vectors X_i are i.i.d. with finite fourth moments, the elements of the matrix product $X_i X_i^T$ have finite variances. Applying the Central Limit Theorem to the vectorized matrix, we find that $\sqrt{t}(\hat{C}_t - C)$ converges in distribution to a zero-mean Gaussian random matrix. Consequently, the Euclidean norm (and thus the operator norm) of the difference is bounded in probability:

$$\|\hat{C}_t - C\|_{op} = O_p(t^{-1/2}) \quad (\text{A.12})$$

Then, by the resolvent identity for invertible matrices A and B , which states $A^{-1} - B^{-1} = -A^{-1}(A - B)B^{-1}$. Setting $A = \hat{C}_t$ and $B = C$, we obtain

$$\Delta_t = \hat{C}_t^{-1} - C^{-1} = -\hat{C}_t^{-1}(\hat{C}_t - C)C^{-1}. \quad (\text{A.13})$$

Taking the operator norm of both sides:

$$\|\Delta_t\|_{op} \leq \|\hat{C}_t^{-1}\|_{op} \|\hat{C}_t - C\|_{op} \|C^{-1}\|_{op}. \quad (\text{A.14})$$

By the Weak Law of Large Numbers, $\hat{C}_t \rightarrow C$ in probability. Since matrix inversion is a continuous function on the manifold of positive definite matrices, $\|\hat{C}_t^{-1}\|_{op} \rightarrow \|C^{-1}\|_{op}$ in probability as well, by the continuous mapping theorem. Therefore, $\|\hat{C}_t^{-1}\|_{op} = O_p(1)$. Substituting the rates gives us

$$\|\Delta_t\|_{op} = O_p(1) \cdot O_p(t^{-1/2}) \cdot O(1) = O_p(t^{-1/2}). \quad (\text{A.15})$$

□

With the above lemma being stated and proved, we rewrite the quadratic form exactly as

$$X_{t+1}^T G_t^{-1} X_{t+1} = \frac{1}{t} X_{t+1}^T (C^{-1} + \Delta_t) X_{t+1} = \frac{1}{t} Z_{t+1} + \frac{1}{t} R_{t+1}, \quad (\text{A.16})$$

where $Z_{t+1} = X_{t+1}^T C^{-1} X_{t+1}$ is the squared Mahalanobis distance, and $R_{t+1} = X_{t+1}^T \Delta_t X_{t+1}$ is the remainder.

Then, using the Taylor expansion $\log(1 + u) = u - \frac{u^2}{2} + O(u^3)$, valid for small u , yields

$$\log \left(1 + \frac{Z_{t+1} + R_{t+1}}{t} \right) = \frac{Z_{t+1}}{t} + \frac{R_{t+1}}{t} - \frac{1}{2} \left(\frac{Z_{t+1}}{t} \right)^2 + O_p \left(\frac{1}{t^3} \right). \quad (\text{A.17})$$

We define $\xi_{t+1} = Z_{t+1} - m$. Note that $\mathbb{E}(Z_{t+1}) = \text{Tr}(C^{-1}C) = m$. Thus $\mathbb{E}(\xi_{t+1}) = 0$ and recall from (3.9) that $\sigma^2 := \text{Var}(Z_{t+1})$. Substituting $Z_{t+1} = m + \xi_{t+1}$:

$$\log \left(1 + \frac{Z_{t+1} + R_{t+1}}{t} \right) = \frac{m + \xi_{t+1}}{t} + \frac{R_{t+1}}{t} - \frac{m^2 + 2m\xi_{t+1} + \xi_{t+1}^2}{2t^2} + O_p \left(\frac{1}{t^3} \right). \quad (\text{A.18})$$

Rearranging the terms by the order of t :

$$\log \left(1 + \frac{Z_{t+1} + R_{t+1}}{t} \right) = \frac{m}{t} + \frac{\xi_{t+1}}{t} + \underbrace{\frac{R_{t+1}}{t} - \frac{m^2}{2t^2}}_{\text{Higher Order Terms}} + O_p \left(\frac{1}{t^{2.5}} \right). \quad (\text{A.19})$$

Summing from n_A to $n - 1$ gives us the decomposition

$$L_n - L_{n_A} = \sum_{t=n_A}^{n-1} \frac{m}{t} + \sum_{t=n_A}^{n-1} \frac{\xi_{t+1}}{t} + \mathcal{E}_{n,n_A}, \quad (\text{A.20})$$

where \mathcal{E}_{n,n_A} is the cumulative error formed by summing over all the higher order terms in (A.19).

To prove the theorem, we remain to examine each component in (A.20). For \mathcal{E}_{n,n_A} , by lemma 4, $R_{t+1} = O_p(t^{-1/2})$ and thus $R_{t+1}/t = O_p(t^{-3/2})$. The summation of R_{t+1} becomes the tail of an absolutely convergent series. Furthermore, standard bias corrections imply this term decays faster than the leading stochastic fluctuation located in the second term, rendering it asymptotically negligible. The entire \mathcal{E}_{n,n_A} will vanish.

For the first summation, using the Euler-Maclaurin expansion $\sum_{t=a}^b \frac{1}{t} = \ln(b) - \ln(a) + O(a^{-1})$ and we have

$$\sum_{t=n_A}^{n-1} \frac{m}{t} = m \ln(n/n_A) + O(n_A^{-1}). \quad (\text{A.21})$$

Finally, for the second summation, the summands ξ_{t+1}/t are independent, centered random variables with variance

$$\text{Var} \left(\frac{\xi_{t+1}}{t} \right) = \frac{\sigma^2}{t^2}. \quad (\text{A.22})$$

The variance of the summation satisfies as $n, n_A \rightarrow \infty$,

$$\text{Var} \left(\sum_{t=n_A}^{n-1} \left(\frac{\xi_{t+1}}{t} \right) \right) = \sum_{t=n_A}^{n-1} \frac{\sigma^2}{t^2} \rightarrow \sum_{t=n_A}^{n-1} \frac{\sigma^2}{t(t+1)} = \sigma^2 \left(\frac{1}{n_A} - \frac{1}{n} \right). \quad (\text{A.23})$$

Combining (A.20), (A.21), (A.23) and the fact \mathcal{E}_{n,n_A} vanishes, we have, by the Central Limit Theorem,

$$\frac{\log \det G_n - \log \det G_{n_A} - m \log(n/n_A)}{\sigma \sqrt{\frac{1}{n_A} - \frac{1}{n}}} \rightarrow \mathcal{N}(0, 1) \quad (\text{A.24})$$

in distribution, as desired. \square

B. Mathematical Details for SIGMA-UB(Section 3.4)

This appendix contains the derivations that connect the theoretical bounds in Section 3.2 to the computable diagnostics in Algorithm 1.

B.1. Regularized log-determinant and PSD Monotonicity

Fix $\delta > 0$. For $X, Y \in \mathbb{S}_+^m$, if $X \preceq Y$ then $X + \delta I_m \preceq Y + \delta I_m$ and

$$\log \det(X + \delta I_m) \leq \log \det(Y + \delta I_m), \quad (\text{B.1})$$

since all eigenvalues are strictly positive after the δI_m shift.

B.2. Diagnostic I: from β_k to a Computable Budget $\widehat{\beta}_k$

Since $G_B^{(k)} \succeq 0$,

$$\beta_k := \lambda_{\max}(G_B^{(k)}) \leq \text{tr}(G_B^{(k)}). \quad (\text{B.2})$$

Using $G_B^{(k)} = \sum_{j \in B} v_j^{(k)} (v_j^{(k)})^\top$ gives

$$\text{tr}(G_B^{(k)}) = \sum_{j \in B} \|v_j^{(k)}\|_2^2. \quad (\text{B.3})$$

Assume preprocessing enforces $\|v_j^{(k)}\|_2^2 \leq \rho$ for all columns. With $n_2 := n_k - n_A$ unseen columns,

$$\beta_k \leq \widehat{\beta}_k := n_2 \rho. \quad (\text{B.4})$$

The above energy cap and tail budget gives us the PSD Majorant (Deterministic Envelope). Indeed, from $G^{(k)} = G_A^{(k)} + G_B^{(k)}$ and Ky-Fan/Weyl dominance,

$$G^{(k)} \preceq G_A^{(k)} + \beta_k I_m \preceq G_A^{(k)} + \widehat{\beta}_k I_m. \quad (\text{B.5})$$

Shifting by δI_m and applying PSD monotonicity yields the valid envelope gives us

$$\log \det(G^{(k)} + \delta I_m) \leq \log \det\left(G_A^{(k)} + (\widehat{\beta}_k + \delta) I_m\right) =: \mathcal{U}_{\text{KF}}^{(k)}(\delta). \quad (\text{B.6})$$

Now let $\mathcal{U}_{\text{KF},*}^{(k)}(\delta) := \log \det(G_A^{(k)} + (\beta_k + \delta) I_m)$. Because $\widehat{\beta}_k \geq \beta_k$, we obtain

$$0 \leq \mathcal{U}_{\text{KF}}^{(k)}(\delta) - \mathcal{U}_{\text{KF},*}^{(k)}(\delta) = \sum_{i=1}^m \log\left(\frac{\lambda_i(G_A^{(k)}) + \widehat{\beta}_k + \delta}{\lambda_i(G_A^{(k)}) + \beta_k + \delta}\right) \leq m \log\left(\frac{\widehat{\beta}_k + \delta}{\beta_k + \delta}\right). \quad (\text{B.7})$$

Rearrange the above inequality and we arrive at the conceptual normalization inequality, which tells us the the gap is controlled by the ideal (incomputable) envelope.

$$\mathcal{U}_{\text{KF}}^{(k)}(\delta) - m \log(\widehat{\beta}_k + \delta) \leq \mathcal{U}_{\text{KF},*}^{(k)}(\delta) - m \log(\beta_k + \delta). \quad (\text{B.8})$$

Motivated by the deduction above, we can define the normalized reporting form as

$$\mathcal{G}_{\text{KF}}^{(k)}(\delta) := \mathcal{U}_{\text{KF}}^{(k)}(\delta) - m \log(\widehat{\beta}_k + \delta), \quad (\text{B.9})$$

which matches (3.16).

B.3. Diagnostic II: LLN Scaling, Cancellation of K , and Covariance Normalization

From the LLN scaling route, we can set

$$\mathcal{U}_{\text{LLN}}^{(k)}(\delta) := \log \det(G_A^{(k)} + \delta I_m) + m \log\left(\frac{n_k}{n_A}\right). \quad (\text{B.10})$$

If $\log \det(G^{(k)}) \leq \log K + \mathcal{U}_{\text{LLN}}^{(k)}(0)$ for an unknown finite K , then baseline differencing removes $\log K$:

$$\Delta \mathcal{U}_{\text{LLN}}^{(k)}(\delta) := \mathcal{U}_{\text{LLN}}^{(k)}(\delta) - \mathcal{U}_{\text{LLN}}^{(0)}(\delta). \quad (\text{B.11})$$

This means that we effectively remove the unknown constant K from the diagnostic. Finally, we can define the covariance-normalized form

$$\mathcal{U}_{\text{LLN},\text{cov}}^{(k)}(\delta) := \mathcal{U}_{\text{LLN}}^{(k)}(\delta) - m \log n_k = \log \det(G_A^{(k)} + \delta I_m) - m \log n_A, \quad (\text{B.12})$$

which is (3.17) and is the statistic computed in Algorithm 1.

B.4. Numerical Computation of log-determinant

For $S \succ 0$, compute $\log \det(S)$ via Cholesky $S = LL^\top$:

$$\log \det(S) = 2 \sum_{i=1}^m \log L_{ii}. \quad (\text{B.13})$$

Apply this to $G_A^{(k)} + \delta I_m$ and $G_A^{(k)} + (\hat{\beta}_k + \delta) I_m$.

C. Supplementary Experiments, Reproducibility, and Extended Diagnostics (FIN)

C.1. Section Roadmap and Artifact Integrity

This section of the appendix serves three purposes.

(i) Reproducibility. We provide a *complete* specification of the experimental pipeline (training, synthetic regeneration, evaluation, and SIGMA-UB computation) in a set of ten self-contained tables (Appendix C.2). The intent is that an external group can rerun the entire loop without relying on implicit conventions.

(ii) Plot-table consistency. All scalar summaries in the main text (final drifts, OLS slopes, and qualitative track agreement) are computed directly from exported per-generation tables. To avoid transcription mistakes, we include the plotted points as tables and (when possible) include them by \input from the auto-exported `tables/*.tex` row files (Appendix C.3). This makes the appendix the *source of truth* for the curves shown in Figures 1–2.

(iii) Additional diagnostics and interpretation. Because SIGMA-UB is a geometric diagnostic (not a surface-form metric), we also report lightweight surface-form proxies—distinct-2 and hashed n -gram HHI—computed on the *same* model outputs used for SIGMA-UB. We include a compact overlay plot that normalizes all signals to $[0, 1]$ to visually assess co-movement (Appendix C.4). We then add a bucket-localization slice (optional) to show where contraction is most pronounced under the frozen prompt taxonomy (Appendix C.5). Throughout, we emphasize that surface-form proxies are *contextual* and not collapse definitions.

Note on filenames. For continuity with earlier drafts, some exported artifact filenames retain the prefix `tech_` (e.g., `tech_s1_two_tracks.pdf`). In this appendix and in the main text, these files correspond to the FIN run described in Section 4.

C.2. Complete reproducibility specification for S1 and S2

We summarize every operational choice that materially affects outcomes: model hyperparameters; synthetic regeneration and mixture; decoding; seeds; SIGMA-UB computation; evaluation metrics; hardware/software; file layout; and the formal difference between S1 and S2. Unless explicitly stated, S1 and S2 share the same configuration; the only intended difference is whether weights are reset to $M^{(0)}$ (S1) or carried forward $M^{(g-1)}$ (S2).

C.3. Exact per-generation values for the main-text drift plots

Figures 1–2 are generated from exported per-generation tables. We include them here to (a) make the plots auditable and (b) guarantee that all reported summary scalars (final drift and OLS slope) can be recomputed from a single canonical source.

Component	S1	S2	Notes
Base model	facebook/opt-125m	facebook/opt-125m	125M parameters
Fine-tuning epochs / gen	5	5	Fixed per-generation budget
Batch size	16	16	Effective batch size held constant
Learning rate	2×10^{-5}	2×10^{-5}	Constant across generations
Optimizer	AdamW	AdamW	Weight decay 0.01
Precision	FP16 enabled	FP16 enabled	GPU training

Table 2. Table 1: Model and training hyperparameters. These hyperparameters are held fixed across S1 and S2 so that observed differences are attributable to *data recursion* vs. *data+weight recursion*, rather than to optimization budget changes.

Item	Value	Applies to	Notes
Real fraction α	0.0 (pure synthetic)	S1, S2	Stress-tests recursion (no real-data anchoring)
Context unit	64 tokens	S1, S2	Training blocks; constant token budget
Real corpus size	$\sim 1,000$ –1,200 contexts / domain	S1, S2	Domain-dependent (DecayBench)
Prompt bank size	~ 163 –200 prompts / domain	Eval	Frozen prompt IDs and bucket labels
Generations reported	$g = 0, \dots, 50$ (51 checkpoints)	Main text	FIN run shown in Figures 1–2
Synthetic pool size	$ S^{(g)} = R $	S1, S2	One synthetic continuation per real context per generation

Table 3. Table 2: Data generation and mixing. We use constant-budget mixtures and, for the reported runs, set $\alpha = 0$ to isolate synthetic recursion dynamics without real-data refresh.

In particular, the S1 vs. S2 summary in Table 1 is computed directly from these per-generation series (including the baseline point $g = 0$, where drift is 0 by definition).

Interpreting Track-I/Track-II disagreement. A recurring pattern in S2 is that Track II indicates strong contraction while Track I does not “collapse” in the same way. This is not a contradiction: Track II measures observed-spectrum log-volume contraction (trend-sensitive), while Track I is an upper-envelope controlled by a worst-case tail-energy budget. When the tail-energy bound is loose relative to the observed sub-Gram spectrum, Track I can be non-alarming even when Track II contracts sharply. In practice, we treat the *separation* itself as informative: it flags “early collapse” regimes where the observed spectrum has contracted but the worst-case envelope remains permissive.

C.4. Surface-form proxy diagnostics and alignment with SIGMA-UB

SIGMA-UB is explicitly designed to track representation geometry rather than surface repetition. Nevertheless, it is useful to ask whether geometry contraction coincides with familiar surface-form failure modes. We therefore compute two lightweight proxies on the *same* generated text used for SIGMA-UB embeddings: (i) distinct-2 (unique/total bigrams; higher is more diverse), and (ii) hashed n -gram HHI (higher is more concentrated/repetitive). These proxies are not collapse definitions and can be noisy, but they provide an operational sanity check.

What the overlay reveals. Figure 3 makes two practical points. First, in S2 the Track-II drift becomes strongly negative early, whereas hashed HHI rises more gradually and can spike later. This indicates that SIGMA-UB Track II can act as an *earlier* indicator of contraction than surface repetition alone. Second, Track I remains near the bottom of the normalized scale in S2 for much of the run, reinforcing that Track I is not intended as a sensitive trend detector; it is a conservative envelope that can remain loose even under clear contraction signals elsewhere.

Endpoint comparison and co-movement. To quantify the qualitative overlay, Table 14 reports proxy endpoints ($g = 0$ vs. $g = 50$) and simple correlation diagnostics between Track II drift and the proxies over generations. The key operational takeaway is that true recursion (S2) yields substantially larger surface-form concentration (HHI increases by nearly three orders of magnitude relative to its $g = 0$ baseline) than restart-from-base (S1), and this increase co-varies strongly with Track II under a rank-based measure.

Full per-generation proxy table (optional). For completeness and auditability, the full per-generation proxy values can be included as a table. This is often useful when debugging changes to tokenization, hashing, or evaluation decoding.

Decoding parameter	Value	Used for	Notes
Sampling type	Nucleus (top- p)	Gen + Eval	Stochastic sampling (not greedy)
Temperature	1.0	Gen + Eval	Fixed across generations
Top- p	0.95	Gen + Eval	Fixed across generations
Max tokens (training)	64	Corpus construction	64-token blocks for training
Max tokens (evaluation)	256	Prompt-bank responses	Used to obtain sufficiently long responses for embedding/geometry

Table 4. Table 3: Text generation (decoding) parameters. Decoding is frozen across checkpoints to prevent evaluation drift and to keep the generation distribution comparable over time.

Aspect	Specification
Base seed	42
Domain offsets	Domain-specific offsets are derived via a deterministic hash (to avoid accidental seed reuse across domains).
Per-context determinism	Synthetic generations are seeded deterministically per real-context ID and generation index.
Per-sample determinism	When multiple sampling steps exist (e.g., batching), the seed schedule ensures reproducible ordering and reproducible stochastic draws.
Implementation note	Seed utility functions are included in the codebase; reruns with the same config reproduce identical synthetic pools and identical evaluation outputs.

Table 5. Table 4: Seeds and determinism. The recursion loop is extremely sensitive to small sampling changes; therefore we enforce determinism at the level of domain, generation, and context ID.

C.5. Within-domain localization by frozen prompt buckets (optional)

Because the evaluation prompt bank is labeled by prompt type (creative, divergent, analogy/ELI5, what-if, neutral), we can localize contraction to specific regimes while keeping the evaluation distribution fixed over time. Concretely, we re-run the evaluation pipeline but restrict to prompts in a single bucket, generating one response per prompt under the same decoding, embedding with the same frozen encoder, and computing the same SIGMA-UB drifts. This is a *slice* of a fixed evaluation set, not a moving target, so it does not introduce evaluation drift.

Interpretation. Bucket localization helps answer a practical question: is contraction uniformly distributed across prompt types, or concentrated where the model is pushed into higher-entropy regimes? In the reported S1 run, the CREATIVE bucket shows consistently larger-magnitude Track-II contraction than the aggregate, suggesting that open-ended prompts amplify the representational narrowing induced by synthetic recursion. That said, bucket series are noisier (and can be non-monotone) because each bucket contains fewer prompts and fewer embedded blocks, so we use them as a diagnostic slice rather than as a headline number.

SIGMA-UB component	Value	Used for	Notes
Sentence encoder	<code>sentence-transformers/all-MiniLM-L6-v2</code>	Embedding	Frozen encoder, $m = 384$
Regularization δ	10^{-3}	Track I/II	Matches Section 3.4 conventions
Energy cap ρ	1.0	Track I	Worst-case tail-energy budget
Baseline	$g = 0$	Drift computation	$\Delta(\cdot)$ reported relative to base checkpoint
Observed block	fixed \mathcal{I}_A within run	Track I/II	Prevents measurement drift across checkpoints

Table 6. **Table 5: SIGMA-UB computation.** Both tracks are computed from the same frozen embeddings and the same observed index set, so drift is attributable to model evolution rather than to evaluation sampling.

Metric family	Reported quantity	Notes
SIGMA-UB Track II	$U_{LLN,cov}$ and $\Delta U_{LLN,cov}$	Sensitive trend probe (observed-spectrum contraction)
SIGMA-UB Track I	G_{KF} and ΔG_{KF}	Conservative envelope; can be loose or non-monotone
Surface proxies	distinct-2, hashed n -gram HHI	Computed on the <i>same</i> generated outputs as SIGMA-UB
Excluded metrics	No perplexity	We intentionally do not report PPL in this revision

Table 7. **Table 6: Evaluation metrics.** The appendix focuses on geometry diagnostics and lightweight surface-form proxies; perplexity-based baselines are excluded by design.

Component	Specification
Training hardware	NVIDIA GPU (server environment)
Metrics hardware	CPU (Mac M1 used for aggregation/plotting)
Core libraries	PyTorch 2.0+, Transformers 4.30+, sentence-transformers 2.2+
Precision	Mixed precision (FP16) enabled during training

Table 8. **Table 7: Computational environment.** Hardware does not change the *definition* of metrics but can affect throughput; determinism is enforced via fixed seeds and fixed decoding.

Artifact	Path template / convention
S1 metrics CSV	<code><METRICS_ROOT>/final/<DOMAIN>/metrics_paper*.csv</code>
S2 metrics CSV	<code><METRICS_ROOT>/true_recursion/<DOMAIN>/metrics_paper_recursion*.csv</code>
Bucket metrics CSV (optional)	<code><METRICS_ROOT>/final/<DOMAIN>/metrics_buckets_paper*.csv</code>
Main-text figures	<code>figures/<prefix>_s1_two_tracks.pdf,</code> <code>figures/<prefix>_s2_two_tracks.pdf</code>
Point tables	<code>tables/<prefix>_s1_two_tracks_points.tex</code> (and S2 analog)
Summary table	<code>tables/tab_<prefix>_s1s2_summary.tex</code>
Surface proxy plot	<code>figures/<prefix>_surface_proxies.pdf</code>

Table 9. **Table 8: Data paths and file structure.** This table documents the exact expected locations of input metrics and the produced figures/tables used by the paper.

Setting	Defining update rule
S1 (restart-from-base)	$M^{(g,d)} \leftarrow \text{Finetune}(M^{(0)}, D^{(g,d)}(\alpha))$. Weights do <i>not</i> compound across generations; only the synthetic data distribution evolves.
S2 (true recursion)	$M^{(g,d)} \leftarrow \text{Finetune}(M^{(g-1,d)}, D^{(g,d)}(\alpha))$. Both synthetic data and weights compound across generations.

Table 10. **Table 9: Key difference between S1 and S2.** This is the core experimental intervention: the regeneration protocol and mixture rule are held fixed while weight carryover is toggled.

Prompt bucket	Description (frozen taxonomy)
Creative	Open-ended creative prompts emphasizing novelty and stylistic variation
Divergent	Prompts encouraging multiple alternatives, brainstorming, or broad exploration
Analogy / ELIS	Prompts asking for analogies, simplifications, or explanatory reframings
What-if	Counterfactual or perturbation prompts (“what if we change X?”)
Neutral	Factual/neutral prompts with minimal stylistic pressure

Table 11. Table 10: Prompt buckets for localization. Bucket IDs and assignments are fixed by DecayBench; slicing by bucket does not change the evaluation distribution over time, it only reveals where contraction is concentrated within a frozen taxonomy.

Generation g	$\Delta U_{\text{LLN},\text{cov}}(\delta)$ (Track II)	$\Delta G_{\text{KF}}(\delta)$ (Track I)	Generation g	$\Delta U_{\text{LLN},\text{cov}}(\delta)$ (Track II)	$\Delta G_{\text{KF}}(\delta)$ (Track I)
0	0.000000	0.000000	26	-136.136651	-127.201498
1	-50.937706	-42.771322	27	-137.363591	-128.428438
2	-87.220752	-78.285600	28	-154.600200	-145.665047
3	-89.193112	-80.257959	29	-134.832965	-125.897812
4	-108.940054	-100.004901	30	-146.391209	-137.456057
5	-138.689852	-130.138891	31	-152.558431	-143.623278
6	-135.146696	-126.211544	32	-126.370288	-117.435135
7	-144.505214	-135.954253	33	-166.712986	-157.777834
8	-158.731260	-149.796107	34	-151.610056	-142.674903
9	-151.887859	-142.952706	35	-158.777897	-149.842744
10	-149.844314	-140.909162	36	-146.721644	-137.786491
11	-171.990854	-163.055701	37	-171.229229	-162.294077
12	-181.172379	-172.237226	38	-145.678374	-136.743222
13	-143.036471	-134.101319	39	-134.396708	-125.461556
14	-146.954698	-138.019546	40	-159.999869	-151.064716
15	-150.025009	-141.089857	41	-151.415048	-142.479895
16	-169.047237	-160.112084	42	-152.343583	-143.408430
17	-134.754288	-125.819136	43	-136.593098	-127.657945
18	-116.984750	-108.049597	44	-140.138527	-131.203374
19	-136.991334	-128.056181	45	-163.640084	-154.704932
20	-135.678684	-126.743532	46	-167.730336	-158.795184
21	-137.759104	-128.823951	47	-138.267815	-129.332663
22	-150.287784	-141.352631	48	-136.290231	-127.355078
23	-154.278070	-145.342917	49	-174.970491	-166.035338
24	-132.792859	-123.857707	50	-150.986188	-142.051035
25	-108.036399	-99.101246			

Table 12. Per-generation values for Figure 1 (S1; restart-from-base). Track II and Track I are reported as drifts relative to the base checkpoint ($g = 0$). In S1, both tracks remain consistently negative at the end of the run ($g = 50$), indicating gradual contraction driven by the evolving synthetic pool even without weight carryover.

Generation g	$\Delta U_{\text{LLN},\text{cov}}(\delta)$ (Track II)	$\Delta G_{\text{KF}}(\delta)$ (Track I)	Generation g	$\Delta U_{\text{LLN},\text{cov}}(\delta)$ (Track II)	$\Delta G_{\text{KF}}(\delta)$ (Track I)
0	0.000000	0.000000	26	-988.967085	1414.089742
1	-51.410418	-1.041078	27	-1033.645644	1337.676319
2	-70.477165	-1.098910	28	-1509.672539	671.355093
3	-67.666663	-1.110627	29	-1520.580241	409.488784
4	-102.965110	-1.173303	30	-1583.494588	323.527521
5	-126.844686	-1.220078	31	-1597.411170	297.547119
6	-156.320891	-1.266556	32	-1514.735790	589.234296
7	-277.027401	-1.665481	33	-1674.100026	139.234670
8	-482.600764	-2.313280	34	-1323.216571	78.225593
9	-586.239077	-2.729119	35	-304.629566	1.402128
10	-589.243534	-2.756645	36	-1284.962201	158.412491
11	-656.250424	-2.917514	37	-1415.459884	151.402919
12	-409.708770	-2.250243	38	-1426.475962	125.709896
13	-366.284030	-2.065401	39	-1773.662017	121.296272
14	-326.883875	-1.910236	40	-2036.524604	221.560576
15	-306.138619	-1.815842	41	-1983.942360	394.404189
16	-266.006178	-1.640532	42	-2191.980469	244.398064
17	-340.097542	-1.858227	43	-2020.929507	145.270029
18	-459.780098	-2.043834	44	-1994.987639	309.382624
19	-580.087915	1920.861134	45	-2028.916186	320.526442
20	-1222.621957	1011.736828	46	-1955.248314	-2.116992
21	-1295.000015	925.612336	47	-1829.693344	3.802502
22	-1369.047226	906.107430	48	-1885.721733	9.290424
23	-985.967065	1455.366376	49	-2000.020743	-1.967390
24	-993.200907	1426.878098	50	-1536.562331	-2.425766
25	-1094.777825	1247.085610			

Table 13. Per-generation values for Figure 2 (S2; true recursion). Track II reaches large-magnitude negative drift (e.g., beyond -1000 by roughly $g \approx 20$ in this run), indicating rapid observed-spectrum contraction under weight carryover. Track I remains near zero and can be non-monotone (including occasional positive excursions), consistent with its role as a conservative envelope controlled by a tail-energy budget rather than by the observed spectrum itself.

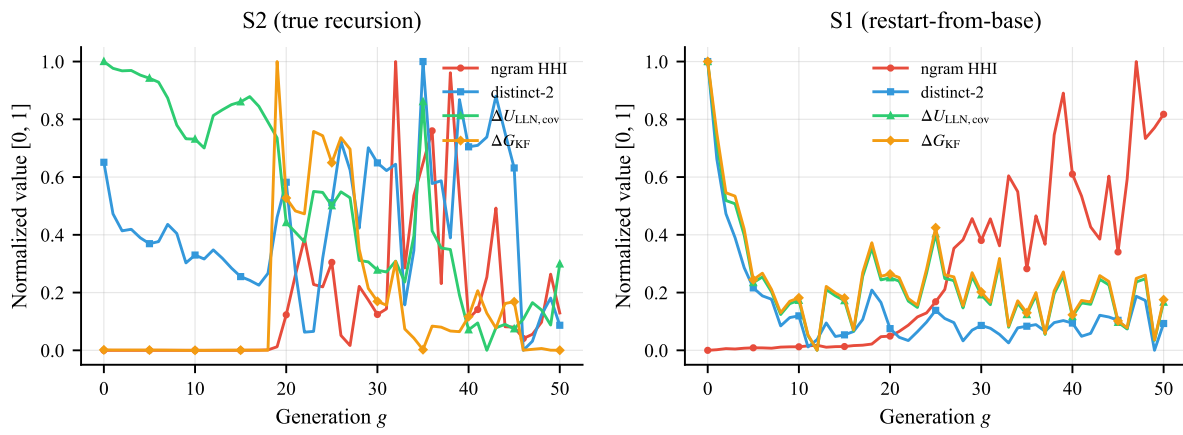


Figure 3. Normalized overlay of SIGMA-UB drifts and surface-form proxies (FIN). Each curve is min–max normalized to $[0, 1]$ within its panel for visual comparability. We overlay four signals across generations: Track II drift $\Delta U_{\text{LLN},\text{cov}}(\delta)$, Track I drift $\Delta G_{\text{KF}}(\delta)$, distinct-2, and hashed n -gram HHI. *Left:* S2 (true recursion). *Right:* S1 (restart-from-base). The key qualitative trend is that the large early Track-II contraction in S2 precedes (and is accompanied by) stronger surface-form concentration (rising HHI) than in S1.

Setting	distinct-2 ($g=0$)	distinct-2 ($g=50$)	HHI ($g=0$)	HHI ($g=50$)	$\text{corr}(\Delta U, \text{distinct-2})$	$\text{corr}(\Delta U, \text{HHI})$	Spearman($\Delta U, \text{HHI}$)
S1	0.731	0.334	0.000102	0.013385	0.926	-0.286	-0.318
S2	0.715	0.254	0.000100	0.097262	-0.165	-0.468	-0.685

Table 14. Surface-proxy alignment with Track II (FIN). Distinct-2 decreases and hashed n -gram HHI increases in both settings, with substantially stronger concentration under true recursion (S2). Correlations are computed over generations using the per-generation series (including $g = 0$). In S1, ΔU and distinct-2 co-move strongly (both decrease), yielding a high positive Pearson correlation. In S2, distinct-2 is noisier (and can transiently increase despite strong contraction), while HHI retains a strong monotone association with ΔU (Spearman ≈ -0.69), consistent with the overlay in Figure 3.

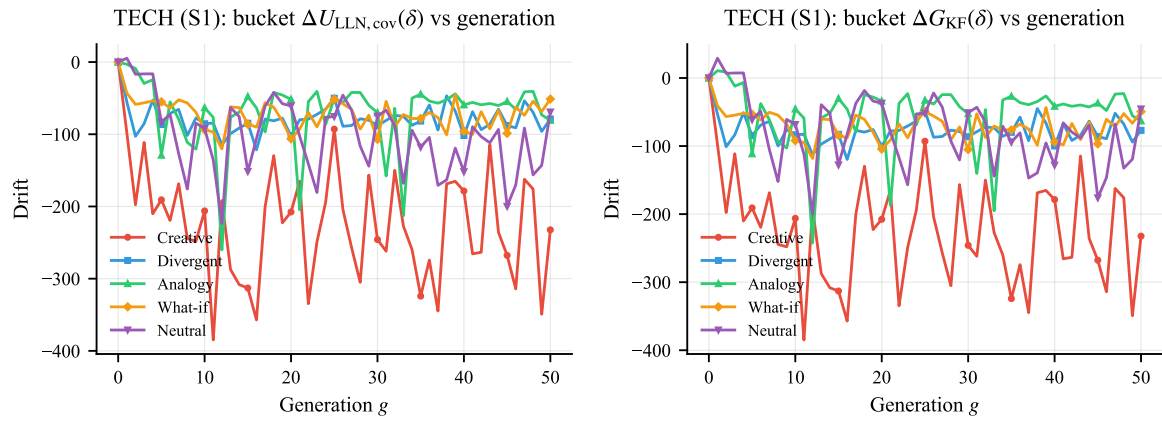


Figure 4. Bucket localization under S1 (FIN; optional). SIGMA-UB drifts computed after restricting evaluation to each frozen prompt bucket. Bucket curves can be noisier than the aggregate because each bucket contains fewer prompts; we therefore interpret bucket localization as a qualitative “where does collapse concentrate?” tool rather than as a primary metric.

g	Creative	Divergent	Analogy/ELI5	What-if	Neutral
0	0.000000	0.000000	0.000000	0.000000	0.000000
1	-97.949065	-55.159718	-3.116045	-42.928381	5.319456
2	-197.646061	-102.878209	-8.989381	-58.633942	-16.935859
3	-111.319080	-85.428164	-29.718339	-56.452165	-16.401600
4	-210.171845	-52.805090	-24.366967	-53.958981	-16.339483
5	-190.844854	-86.526231	-129.090423	-55.162083	-83.129598
6	-219.455934	-71.041283	-55.255710	-63.533863	-72.571280
7	-168.494531	-65.564080	-79.075972	-52.309351	-126.984507
8	-244.501580	-101.711687	-111.373454	-56.608878	-175.909325
9	-248.006326	-77.422012	-120.572586	-69.700436	-84.569910
10	-206.202956	-85.442737	-63.331140	-93.868086	-92.089470
11	-384.826592	-84.560220	-76.590153	-96.869445	-135.712099
12	-191.844812	-114.666577	-260.148545	-120.239236	-223.771048
13	-287.341241	-99.117427	-76.357705	-62.108385	-63.006851
14	-308.242176	-91.501159	-69.393513	-63.105835	-75.480431
15	-312.938055	-84.708643	-47.853525	-86.176912	-151.496944
16	-357.149831	-121.594475	-63.509059	-90.049027	-106.138078
17	-200.374851	-78.959020	-96.759571	-56.453774	-61.019787
18	-129.635475	-81.399424	-42.033181	-62.702197	-42.118850
19	-222.708576	-77.688492	-45.745484	-81.863135	-57.727289
20	-207.613162	-102.415834	-51.668224	-106.350109	-60.770080
21	-165.012269	-79.875531	-204.677032	-93.085949	-102.880295
22	-334.643279	-79.037445	-54.864907	-69.461680	-140.839753
23	-248.946713	-72.418699	-40.687391	-89.783746	-180.663248
24	-194.390032	-65.316534	-86.586005	-64.861563	-76.556536
25	-92.896077	-50.135445	-50.367304	-51.637901	-75.460966
26	-204.110634	-88.983083	-55.942330	-57.759885	-45.832592
27	-256.717613	-87.868162	-42.095798	-65.592657	-66.432976
28	-305.102122	-78.531429	-42.149740	-92.922173	-116.332023
29	-156.620419	-80.583804	-59.878911	-73.651079	-144.240864
30	-245.838960	-88.216022	-70.145223	-107.060914	-74.803194
31	-261.953853	-80.824331	-157.886675	-54.458516	-66.717892
32	-150.001326	-73.853490	-64.132656	-89.356801	-88.258118
33	-227.135310	-75.126110	-212.806264	-72.637732	-167.992962
34	-259.798832	-87.601284	-49.906544	-78.191872	-94.565098
35	-324.139874	-81.799765	-44.590636	-78.285666	-117.771632
36	-274.266735	-59.455086	-53.930531	-69.795271	-104.338444
37	-344.774439	-94.113630	-56.990416	-76.943106	-170.769428
38	-168.644537	-46.805503	-52.271075	-100.768563	-163.202054
39	-165.214096	-68.054030	-44.045319	-45.225875	-119.155531
40	-178.614273	-101.818107	-59.327405	-95.767226	-151.824765
41	-265.623322	-68.819743	-55.908253	-100.310327	-89.635536
42	-263.447148	-93.701634	-59.242546	-68.744265	-103.269554
43	-114.642464	-85.956916	-57.339421	-92.521798	-111.816243
44	-235.803806	-65.343599	-60.264987	-66.722845	-93.284889
45	-267.718776	-87.940112	-54.625358	-98.657337	-199.815871
46	-314.117762	-91.077680	-65.452508	-62.377067	-170.152065
47	-162.290329	-53.746197	-41.316406	-73.824375	-91.395436
48	-175.864254	-69.564232	-40.553158	-54.144934	-156.291398
49	-349.254658	-96.036588	-73.186376	-68.534576	-143.092325
50	-232.342407	-78.865678	-80.803164	-51.253275	-69.202759

Table 15. Track-II drift by bucket under S1 (FIN; optional). Each entry is $\Delta U_{LLN, \text{cov}}(\delta)$ computed using only prompts from the given bucket (baseline $g = 0$). In this run, CREATIVE tends to exhibit the largest-magnitude negative drift by late generations, while other buckets are comparatively less contracted. Because bucket sizes differ, cross-bucket comparisons should be interpreted qualitatively unless normalized for prompt count.